© 2019. Published by The Company of Biologists Ltd | Development (2019) 146, dev169219. doi:10.1242/dev.169219

RESEARCH ARTICLE

Targeted substrate degradation by Kelch controls the actin cytoskeleton during ring canal expansion

Andrew M. Hudson[1,‡], Katelynn M. Mannix[1,‡], Julianne A. Gerdes[1], Molly C. Kottemann[1,*] and Lynn Cooley[1,2,3,§]

ABSTRACT

During *Drosophila* oogenesis, specialized actin-based structures called ring canals form and expand to accommodate growth of the oocyte. Previous work demonstrated that Kelch and Cullin 3 function together in a Cullin 3-RING ubiquitin ligase complex (CRL3^{Kelch}) to organize the ring canal cytoskeleton, presumably by targeting a substrate for proteolysis. Here, we use tandem affinity purification followed by mass spectrometry to identify HtsRC as the CRL3^{Kelch} ring canal substrate. CRISPR-mediated mutagenesis of HtsRC revealed its requirement in the recruitment of the ring canal F-actin cytoskeleton. We present genetic evidence consistent with HtsRC being the CRL3^{Kelch} substrate, as well as biochemical evidence indicating that HtsRC is ubiquitylated and degraded by the proteasome. Finally, we identify a short sequence motif in HtsRC that is necessary for Kelch binding. These findings uncover an unusual mechanism during development wherein a specialized cytoskeletal structure is regulated and remodeled by the ubiquitin-proteasome system.

KEY WORDS: *Drosophila* oogenesis, Ring canal, Cullin 3, Kelch, Ubiquitin-proteasome system, Actin cytoskeleton

INTRODUCTION

Drosophila oogenesis provides a powerful model for investigating the specialized features of gamete development (Bastock and St Johnston, 2008). Female fruit flies produce up to 60 eggs per day, each ∼0.5 mm in length with a volume more than 1000-fold greater than that of a typical somatic cell. Oogenesis initiates at the anterior end of an ovariole, called the germarium, where a daughter of a germline stem cell undergoes four rounds of mitosis to generate a 16-cell cyst. One of these cells becomes the oocyte, while the remaining 15 differentiate as nurse cells. Cytokinesis does not complete during the mitotic divisions, leaving all 16 cells connected by the arrested cleavage furrows. The arrested cleavage furrows become stable intercellular bridges called ring canals through the recruitment of additional proteins (Haglund et al., 2011). Over the course of several days, the nurse cells become highly polyploid and synthesize mRNA, protein and organelles that support oocyte growth. These components move to the oocyte through the ring canals, which recruit a robust F-actin cytoskeleton and expand during oogenesis to accommodate the flux of materials.

An important mechanism for regulating developmental events during gametogenesis is the ubiquitin-proteasome system (UPS). Covalent attachment of ubiquitin to a target protein can alter the fate of the protein in a number of ways (Komander and Rape, 2012). Mono-ubiquitylation, the attachment of a single ubiquitin, can serve as a signal for endocytic sorting. When lysine 48-linked chains of ubiquitin are attached, the ubiquitylated protein is targeted for destruction by the proteasome. Protein ubiquitylation is carried out by three enzymes acting in sequence, termed E1, E2 and E3. Substrate specificity is conferred by the E3 enzyme, and several classes of E3 enzymes have been characterized. Genes encoding E3 enzymes have undergone significant expansion in higher eukaryotes such that 3% of human genes (>600 out of 20,000) encode substrate-specific E3 enzymes (Li et al., 2008).

BTB-BACK-Kelch (BBK) proteins function as substrate adaptors for a class of ubiquitin E3 ligases called Cullin 3-RING ubiquitin ligases (CRL3s) (Fig. 1A) (Xu et al., 2003). The elongated Cullin 3 (Cul3) protein binds a BTB-domain protein at its N terminus and a RING domain protein at its C terminus. The RING domain recruits an E2 ubiquitin-conjugating enzyme, whereas the BTB-domain protein recruits specific substrates for ubiquitylation through its C-terminal Kelch-repeat domain (KREP), which adopts a β-propeller structure (Adams et al., 2000; Li et al., 2004). The BBK gene family has undergone significant expansion during animal evolution; the *Drosophila* genome encodes ∼10 BBK proteins, whereas nearly 50 distinct BBK genes are present in humans (Dhanoa et al., 2013; Prag and Adams, 2003). Mutations in human BBK genes are associated with a number of diseases, including cancer, neurodegenerative disease, infertility and congenital skeletal myopathies, underscoring their clinical importance (Bomont et al., 2000; Gupta and Beggs, 2014; Padmanabhan et al., 2006; Yatsenko et al., 2006). A common thread suggested by these disease associations is BBK-mediated regulation of metazoan-specific cytoskeletal structures. Studying the targets of BBK/CRL3 ubiquitylation therefore requires access to experimental systems amenable to analysis of cytoskeletal regulation.

We have previously demonstrated that *Drosophila* Kelch functions with Cullin 3 to coordinate the growth of the ovarian ring canal cytoskeleton during oogenesis (Hudson and Cooley, 2010; Hudson et al., 2015). Here, we present evidence that HtsRC, one product of the *hts* gene, is the key substrate of CRL3^{Kelch} required for ordered ring canal expansion during egg chamber growth. We identified HtsRC as a potential substrate of CRL3^{Kelch} based on its association with the KREP domain, and we identified a candidate Kelch-binding site in HtsRC responsible for targeting by CRL3^{Kelch}. Disruption of this motif by gene editing resulted in a ring canal phenotype identical to *kelch*. We demonstrated that

[1]Department of Genetics, Yale University School of Medicine, New Haven, CT 06520, USA. [2]Department of Cell Biology, Yale University School of Medicine, New Haven, CT 06520, USA. [3]Department of Molecular, Cellular & Developmental Biology, Yale University, New Haven, CT 06520, USA.
*Present address: Laboratory of Genome Maintenance, The Rockefeller University, New York, NY 10065, USA.

‡These authors contributed equally to this work

§Author for correspondence (lynn.cooley@yale.edu)

A.M.H., 0000-0002-2880-2051; K.M.M., 0000-0003-4541-5050; J.A.G., 0000-0002-4691-1331; L.C., 0000-0003-4665-1258

Received 4 September 2018; Accepted 27 November 2018

Development (2019) 146, dev169219. doi:10.1242/dev.169219

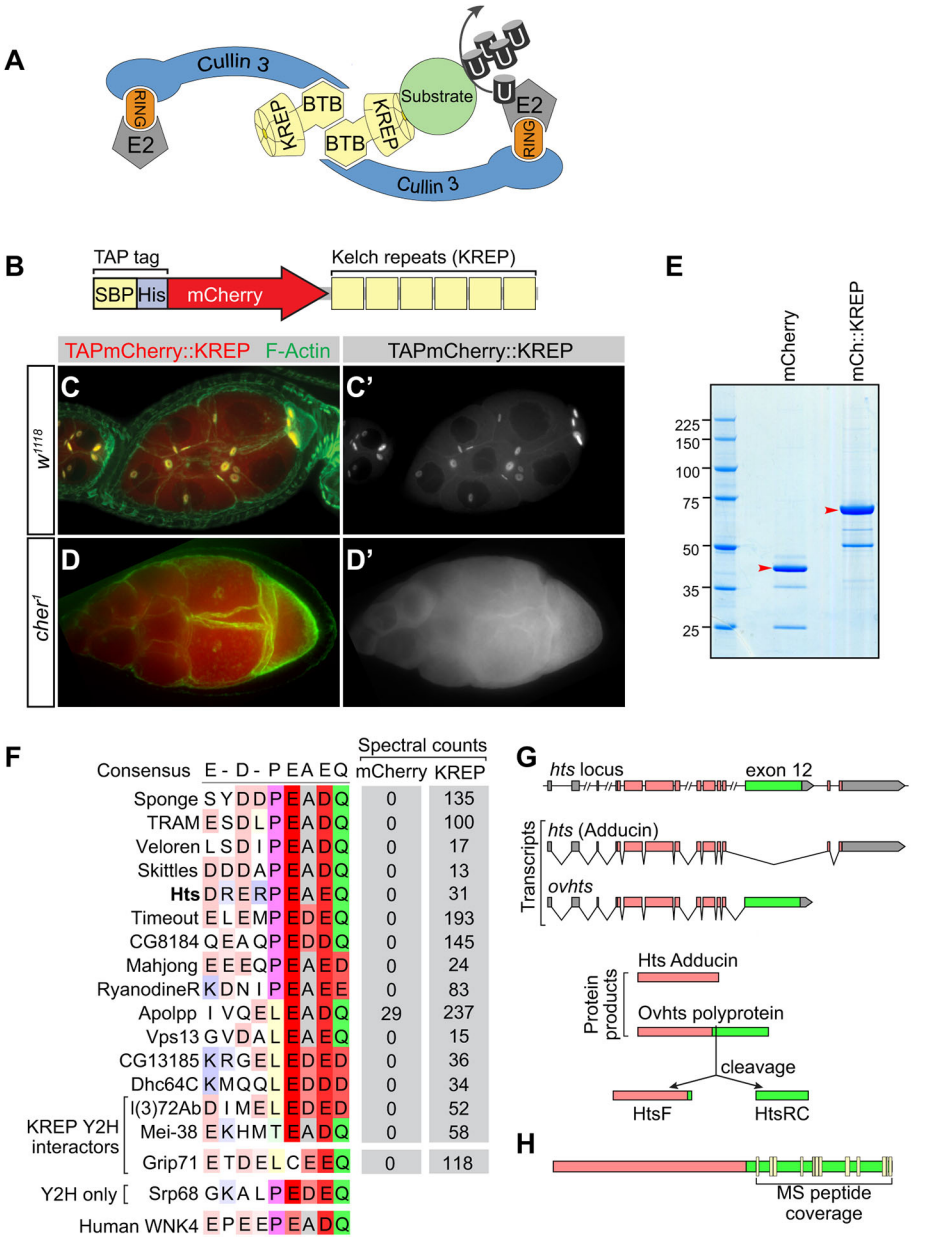

Fig. 1. Tandem affinity purification and mass spectrometry reveals HtsRC as a potential CRL3^{Kelch} substrate. (A) Cartoon of a CRL3^{Kelch} dimer, showing ubiquitylation of a substrate (green circle). (B) Diagram of TAP-tagged mCherry fused to the Kelch KREP domain. (C,C′) High-level expression of the mCherry::KREP fusion using the *matGal4* driver resulted in ring canal localization and a dominant *kelch*-like phenotype. (D,D′) In *cher*^{1} mutant ovaries, the mCherry::KREP fusion exhibited a homogeneous cytosolic distribution and was not associated with ring canals. (E) Proteins bound to TAP-tagged mCherry or TAPmCherry::KREP were purified from *cher*^{1} mutant ovaries, separated on a 4-12% SDS-PAGE gel, stained with colloidal Coomassie and subjected to LC-MS/MS. Purified TAPmCherry and TAPmCherry::KREP proteins are indicated by red arrowheads. (F) Sequence analysis of proteins bound specifically to TAPmCherry::KREP that contain a motif consisting of several acidic residues followed by a PEAEQ consensus sequence defined by the expression [PLT]-E-[AD]-[DE]-[QD]. Sequences were manually aligned in JalView (Waterhouse et al., 2009). (G) Alternative splicing of *hts* transcripts produces several mRNAs, including mRNAs encoding Adducin. The ovary-specific *ovhts* mRNA contains exon 12 (green) and produces a polyprotein that is cleaved to produce truncated Adducin (HtsF) that localizes to fusomes and the novel HtsRC protein that localizes to ring canals. (H) Peptides identified from proteins bound to mCherry::KREP mapped entirely to HtsRC (yellow boxes). See also Figs S1, S2 and Table S1.

HtsRC can be ubiquitylated and degraded by the proteasome in cultured cells and in ovaries. Finally, we carried out a series of genetic interaction experiments that further support the conclusion that HtsRC is the substrate of CRL3^{Kelch} in ring canals.

RESULTS

Tandem affinity purification and mass spectrometry reveals HtsRC as a potential CRL3^{Kelch} substrate

Egg chambers from *Drosophila* females mutant for *kelch* have ring canals with a highly disorganized F-actin cytoskeleton that impedes the flow of cytoplasm to growing oocytes (Xue and Cooley, 1993). We have reported that Kelch functions as the substrate-targeting component of a Cullin-RING E3 ubiquitin ligase (CRL3^{Kelch}) and that its CRL activity is essential for ring canal cytoskeletal organization (Hudson and Cooley, 2010; Hudson et al., 2015). To understand the role of Kelch in ring canal morphogenesis, we sought to identify substrates of CRL3^{Kelch}. We have previously shown that overexpression of the KREP domain results in a *kelch*-like dominant-negative phenotype (Fig. 1C), marked by the accumulation of KREP at the ring canal (Hudson and Cooley, 2010). This phenotype suggested that the KREP domain might be bound to its substrate in a stable complex lacking Cul3 that cannot promote substrate ubiquitylation. We therefore used affinity purification of the KREP domain to identify potential substrates by mass spectrometry.

We expressed TAP-tagged mCherry::KREP (Fig. 1B) and a TAP-tagged mCherry control in ovarian germ cells. However, initial experiments were hindered by the poor solubility of ring canal components lysed under conditions that would preserve protein-protein interactions. We therefore performed purifications in a mutant background to liberate ring canal components from the insoluble cytoskeleton. *cheerio* (*cher*) encodes *Drosophila* Filamin (Sokol and Cooley, 1999). In *cher* mutants, ring canals lack the robust F-actin cytoskeleton found in wild type (Fig. 1C,D) and Kelch fails to properly localize despite being present in ovarian lysates (Robinson et al., 1997). We performed parallel purifications of mCherry or mCherry::KREP from *cher* mutant females (Fig. 1E) and identified co-purifying proteins by mass spectroscopy.

Development (2019) 146, dev169219. doi:10.1242/dev.169219

From nearly 900 proteins identified in the KREP purification, we focused on 141 candidate substrates based on specificity of interaction and relative abundance (approximated by total spectral counts; see Table S1).

Sequence analysis of the candidate substrates revealed that they were enriched for proteins containing a short linear sequence motif consisting of several acidic residues followed by a consensus PEAEQ sequence (15 out of 141; $P=8\times10^{-8}$, binomial test) (Fig. 1F). A similar motif is also present in three human WNK kinases targeted by KLHL3, a human ortholog of Kelch (Boyden et al., 2012; Shibata et al., 2013). These results suggest that the PEAEQ motif is a binding site for Kelch and closely related BBK proteins. In further support of this idea, we identified four PEAEQ-containing proteins in a yeast two-hybrid screen for KREP domain interactors, and all cDNAs isolated contained the regions encoding the PEAEQ motif (Fig. S1).

Several PEAEQ proteins identified by mass spectrometry have known functions in F-actin assembly and organization, including Hts (Fig. 1F). The *hts* locus encodes multiple proteins, including conserved and ubiquitously expressed isoforms of the cytoskeletal protein Adducin (Fig. 1G) (Yue and Spradling, 1992). In the ovary, a germline-specific transcript designated *ovhts* encodes a polyprotein that is cleaved to produce two distinct products: an Adducin isoform that localizes to the fusome within mitotic cells (referred to as HtsF) and the novel Hts ring canal (HtsRC) polypeptide that localizes to germline ring canals (Fig. 1G) (Petrella et al., 2007). All of the Hts peptides identified by mass spectrometry mapped to the HtsRC part of Ovhts (Fig. 1H), suggesting that the ring canal protein, and not an Adducin isoform, was associated with the KREP domain. Sequence analysis of other *Drosophila* species revealed that the HtsRC PEAEQ sequence is invariant, whereas adjacent sequences show less conservation, suggesting a functional role for this sequence (Fig. S2). We therefore sought to determine whether HtsRC is a substrate of $CRL3^{Kelch}$.

HtsRC is ubiquitylated and degraded by the proteasome

To assess HtsRC ubiquitylation, we expressed HtsRC in cultured S2 cells by cloning exon 12 (see Fig. 1G) into an expression vector with HA epitope tags at both the N and C termini (Fig. 2A). We reasoned that transfected HtsRC should be regulated by $CRL3^{Kelch}$ as all components of the $CRL3^{Kelch}$ ubiquitin ligase machinery are present. S2 cells produced both 3xHA::HtsRC::HA precursor protein and the HtsRC::HA cleavage product with no N-terminal tag (Fig. 2A). Cells were treated with DMSO (control) or 1 µM bortezomib, a proteasome inhibitor, for 3 and 6 h. Whole-cell lysates analyzed by western blotting showed that proteasome

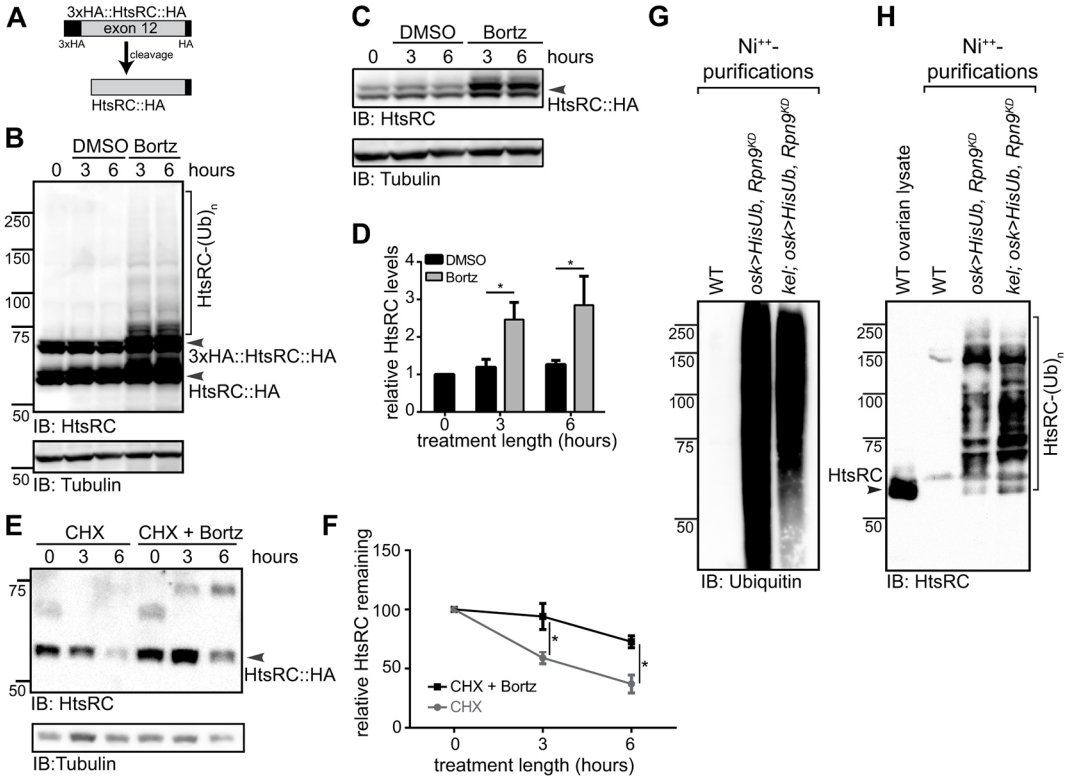

Fig. 2. HtsRC is ubiquitylated and degraded by the proteasome. (A) Cartoon showing full-length 3xHA::HtsRC::HA and cleaved HtsRC::HA protein products. (B) S2 cells expressing 3xHA::HtsRC::HA were treated with DMSO (control) or 1 µM bortezomib for 3 or 6 h, 24 h post-transfection, lysed and analyzed by western blotting. Proteasome inhibition results in higher molecular weight, presumably ubiquitylated, HtsRC species. (C) S2 cells were treated with DMSO (control) or 1 µM bortezomib for 3 and 6 h, 36 h post-transfection, lysed and analyzed by western blotting. (D) Levels of HtsRC::HA were elevated after bortezomib treatment. *P<0.05; Student's t-test. Data are from three independent experiments. (E) Cells expressing 3xHA::HtsRC::HA 24 h post-transfection were treated with 100 µg/ml cycloheximide (CHX) with or without 1 µM bortezomib, harvested at 3 and 6 h timepoints, and analyzed by western blotting. (F) Quantification of HtsRC protein levels from three independent CHX chase experiments. HtsRC protein levels decreased after CHX treatment and were stabilized with bortezomib treatment, suggesting that HtsRC is degraded by the proteasome. *P<0.05; Student's t-test. (G) Blots of proteins eluted from Ni^{++}-NTA purifications from control ovary extracts lacking His::Ub, and wild-type or $kelch^{DE1}$ mutant extracts expressing His::Ub. Anti-ubiquitin antibody P4D1 revealed strong and specific enrichment of ubiquitylated proteins in purifications from His::Ub extracts. (H) Blot of total ovarian protein (lane 1) and proteins eluted from Ni^{++}-NTA purifications as in G. Anti-HtsRC antibody revealed a ladder of ubiquitylated HtsRC species in His::Ub purifications from both wild-type and *kelch* mutant extracts. Two minor cross-reacting bands eluted from Ni^{++}-NTA beads in wild-type extracts were recognized by HtsRC in the control.

Development (2019) 146, dev169219. doi:10.1242/dev.169219

inhibition resulted in a higher molecular weight, presumably ubiquitylated, HtsRC species (Fig. 2B). Proteasome inhibition also resulted in a twofold increase of HtsRC protein compared with DMSO control (Fig. 2C,D).

We tested HtsRC stability upon proteasome inhibition in the context of inhibiting new protein synthesis with cycloheximide (Fig. 2E,F). In cycloheximide-treated S2 cells, HtsRC levels declined over 6 h. With addition of proteasome inhibition, HtsRC declined more slowly (Fig. 2E,F). These data suggest that HtsRC is degraded by the proteasome in cultured *Drosophila* cells.

To determine whether endogenous HtsRC is ubiquitylated, we developed an assay to monitor protein ubiquitylation in ovarian germ cells. We used the germline-specific *oskGal4* driver to express His-tagged Ubiquitin in combination with an shRNA targeting the proteasome subunit *Rpn9*. Knockdown of *Rpn9* results in a moderate reduction of proteasome activity and was included to enrich for ubiquitylated proteins. We purified His-tagged proteins from wild type and *oskGal4>His::Ub, Rpn9*^{KD} ovaries, and observed a clear enrichment of ubiquitylated proteins in the HisUb samples (Fig. 2G), indicating that we could efficiently isolate ubiquitylated proteins. HtsRC was detected as a high molecular weight series of bands in purifications from His::Ub-expressing flies, indicating that HtsRC is a ubiquitylated protein in ovarian germ cells (Fig. 2H). We note that *Rpn9* knockdown does not affect the processing of the Ovhts polyprotein (Fig. S3), eliminating the possibility that some of these bands could be partially processed forms of the Ovhts polyprotein. To determine whether ubiquitylation of HtsRC was dependent on the presence of Kelch, we performed a parallel experiment using flies lacking Kelch. To our surprise, we also detected HtsRC among the ubiquitylated proteins purified from *kelch* mutant lysates, with no apparent reduction in intensity relative to wild type (Fig. 2H). These results demonstrate that HtsRC is ubiquitylated in ovarian germ cells, but also reveal that the activity of CRL3^{Kelch} is not the only pathway leading to HtsRC ubiquitylation in these cells. We therefore turned to genetic experiments to determine whether CRL3^{Kelch} targets HtsRC specifically at the ring canal.

Altered HtsRC expression can suppress or enhance the *kelch*-like ring canal phenotype

We performed a series of genetic enhancement and suppression experiments to determine how HtsRC protein expression levels affect the *kelch*-like ring canal phenotype caused by germline-specific proteasome inhibition (Fig. 3A). Ring canal F-actin thickness was assessed using the full width at half max (FWHM) measure of F-actin intensity plots. We analyzed ring canals from stage 6 egg chambers for this analysis because proteasome inhibition caused egg chamber arrest and degeneration beyond this stage (Hudson et al., 2015). Germline-specific expression of shRNAs targeting ProsBeta5, a catalytic subunit of the proteasome, led to *kelch*-like ring canals (Fig. 3A, red), marked by significantly thicker ring canal F-actin compared with wild-type ring canals (Fig. 3A, black). Increased HtsRC::GFP expression, achieved by expressing a *UASH-ovhts::GFP* construct (Petrella et al., 2007), significantly enhanced the *kelch*-like ring canal phenotype observed upon proteasome inhibition (Fig. 3A, green). Additionally, removal of one copy of *kelch* in the context of proteasome inhibition and HtsRC::GFP expression further increased the ring canal F-actin thickness (Fig. 3A, yellow). Conversely, removal of one copy of *htsRC* (achieved via CRISPR-mediated mutagenesis of the HtsRC-encoding exon; see Fig. 4A,F-G‴) was sufficient to suppress the *kelch*-like ring canal phenotype caused by proteasome inhibition (Fig. 3A, blue). These results reveal that increased or decreased HtsRC expression can significantly enhance or suppress, respectively, the *kelch*-like ring canal F-actin phenotype caused by proteasome inhibition, and that HtsRC, Kelch and the proteasome genetically interact.

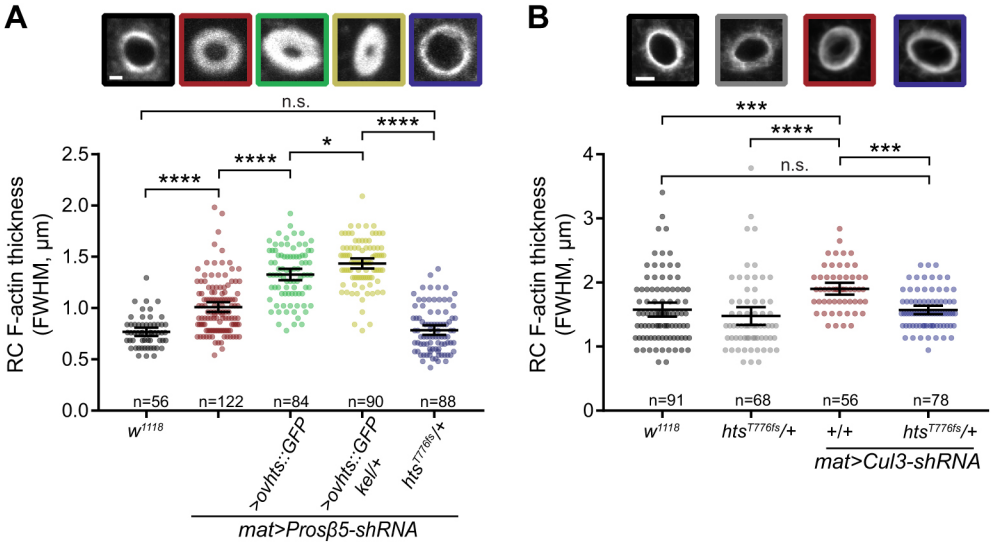

Fig. 3. Altered HtsRC expression can suppress or enhance the *kelch*-like ring canal phenotype. (A,B) Ring canal F-actin thickness in stage 6 (A) or stage 9 (B) egg chambers was calculated using the full width at half max (FWHM) measure of F-actin intensity plots spanning across ring canals. Colored boxed images show representative ring canals of each genotype, with corresponding individual data points below for each ring canal measured. Bars represent the F-actin thickness as mean±95% confidence interval. *n* denotes number of ring canals measured. (A) Increased or decreased HtsRC expression enhanced or suppressed, respectively, the *kelch*-like ring canal phenotype observed upon germline-specific proteasome inhibition by RNAi. Proteasome inhibition led to *kelch*-like ring canals, marked by significantly thicker F-actin rings (red). Increased HtsRC::GFP expression (green) and increased HtsRC::GFP expression with loss of one copy of *kelch* (yellow) significantly increased ring canal F-actin thickness, whereas removal of one copy of *htsRC* fully suppressed the *kelch*-like phenotype observed upon proteasome inhibition (blue). Scale bar: 1 µm. (B) Germline-specific knockdown of *Cul3* by RNAi led to *kelch*-like ring canals (red), marked by significantly thicker F-actin rings. Removal of one copy of *htsRC* was sufficient to suppress the *kelch*-like phenotype (blue). ****P<0.0001, ***P<0.001, *P<0.05; one-way ANOVA, Tukey's multiple comparison test. n.s., not significant. Scale bar: 2 µm.

Development (2019) 146, dev169219. doi:10.1242/dev.169219

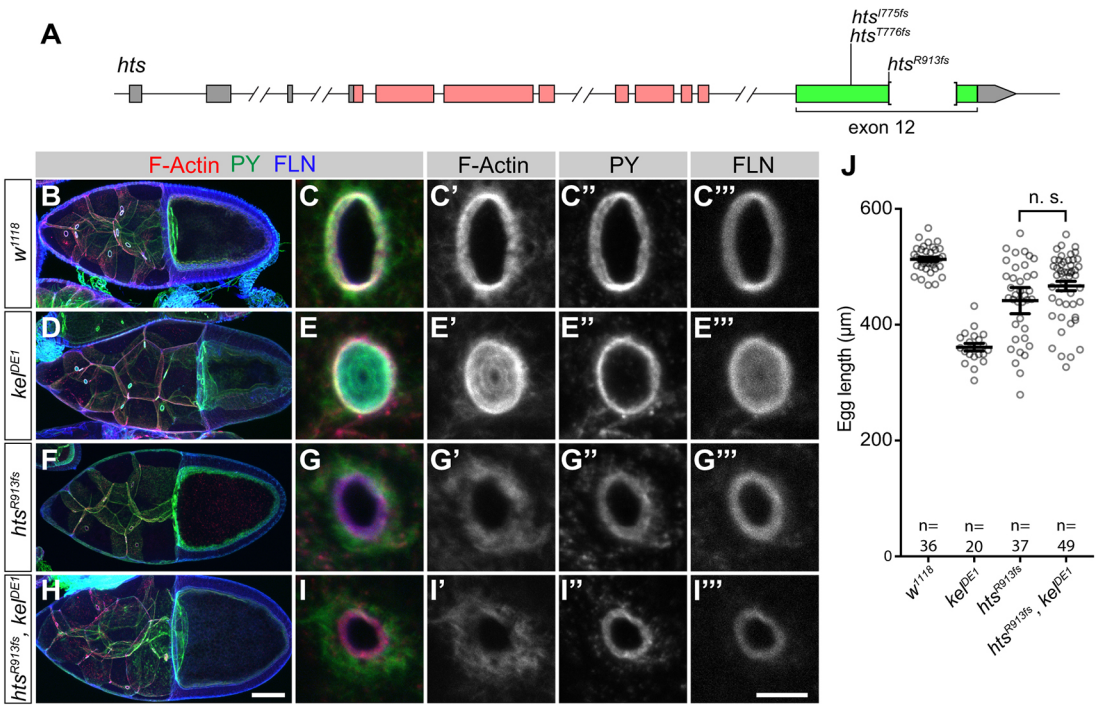

Fig. 4. Genetic analysis indicates *hts* is epistatic to *kelch*. (A) Diagram summarizing the locations of CRISPR/NHEJ-induced deletion mutations in *hts* exon 12. hts^{I775fs} is a 2 bp deletion (Chr2R:19401008…19401009, FlyBase release 6); translation of the mutant cDNA would produce a 62 amino acid extension in the new reading frame starting at I775 of Ovhts. hts^{T776fs} is a single base pair deletion (Chr2R:19401007) resulting in a frameshift extension of 28 amino acids beginning at T776. hts^{R913fs} is a 559 bp deletion (Chr2R:19400036…19400594) resulting in a frameshift extension of 10 amino acids beginning at R913, immediately prior to the DRERPEAEQ sequence. (B,D,F,H) Wild-type, kel^{DE1}, hts^{R913fs} and hts^{R913fs}, kel^{DE1} stage 10 egg chambers showing the distributions of F-actin, phosphotyrosine (PY) and Filamin (FLN). *kelch* mutant egg chambers displayed a fully penetrant 'small oocyte' phenotype at stage 10 (D). Oocytes in hts^{R913fs} (F) and hts^{R913fs}, kel^{DE1} double mutant egg chambers (H) did not exhibit a penetrant stage 10 growth defect. (C-C‴,E-E‴,G-G‴,I-I‴) High-resolution images of ring canals from the genotypes indicated. $kel^{DE1}$and hts^{R913fs} ring canals exhibited opposite phenotypes with respect to ring canal F-actin accumulation: excess F-actin in kel^{DE1} and only a small amount of peripheral F-actin accumulation around the ring canals in the hts^{R913fs} mutant. Scale bars: 50 µm in H; 5 µm in I‴. (J) Quantification of egg lengths from the indicated genotypes. The hts^{R913fs}, kel^{DE1} double mutant phenotype was indistinguishable from hts^{R913fs}, demonstrating that *hts* is epistatic to *kelch*. Bars represent egg length as mean±95% confidence interval. One-way ANOVA, Tukey's multiple comparison test; n.s., not significant. See also Fig. S4.

We also tested the ability of HtsRC expression to affect the ring canal F-actin organization in stage 9 control egg chambers or egg chambers experiencing germline-specific knockdown of *Cul3* (Fig. 3B). As shown previously (Hudson et al., 2015), knockdown of *Cul3* leads to *kelch*-like ring canals (Fig. 3B, red). Removal of one copy of *htsRC* was sufficient to fully rescue this phenotype (Fig. 3B, blue). These data show that alteration of HtsRC protein levels can enhance and suppress the *kelch*-like ring canal F-actin phenotype in multiple contexts.

Genetic analysis indicates *hts* is epistatic to *kelch*

Functional analyses of HtsRC have been limited due to the multiple requirements for *hts* during oogenesis, including both germline mitotic divisions and oocyte specification (Yue and Spradling, 1992; Petrella et al., 2007). To determine the consequence of specifically disrupting HtsRC expression, we used CRISPR/Cas9 non-homologous end-joining (NHEJ) mutagenesis to introduce frameshift mutations in the exon encoding HtsRC (Figs 1G and 4A, green). We isolated three frameshift alleles that result in premature truncation of HtsRC (Fig. 4A). These alleles exhibited similar phenotypes whether homozygous or in trans to a deficiency, and none produced detectable HtsRC by immunofluorescence (Fig. S4E,E′) or immunoblot (Fig. S5A) analyses, indicating that they are strong loss-of-function alleles. Ovaries from these mutant females exhibited none of the germline mitotic defects associated with alleles affecting the Adducin isoforms. The fusome was present with Adducin localization indistinguishable from wild type (Fig. S4). Instead, the *htsRC* alleles displayed a specific ring canal phenotype, in which the robust inner rim of F-actin was absent (Fig. S4 and Fig. 4F,G′). We note that the *htsRC*-specific actin phenotype could be rescued by expression of Ovhts::GFP (Fig. S4). Consistent with previous work (Sokol and Cooley, 1999), Filamin was detectable at these ring canals (Fig. 4G‴), confirming that Filamin localization to ring canals is independent of HtsRC.

The loss-of-function phenotypes of *kelch* and *htsRC* were opposite of one another: in *htsRC*-specific mutants, ring canals lacked F-actin (compare Fig. 4C′ with 4G′; only peripheral subcortical F-actin is present in G′), whereas in *kelch* mutant females the F-actin cytoskeleton accumulated aberrantly in the ring canal lumens (Fig. 4E′). We examined double mutant combinations of loss-of-function alleles kel^{DE1} and hts^{R913fs}. The double mutant was identical to the hts^{R913fs} single mutant with regard to the ring canal F-actin (Fig. 4F-I) and oocyte size phenotype (Fig. 4J), demonstrating that hts^{R913fs} is epistatic to *kelch*. This is consistent with HtsRC being an important substrate of $CRL3^{Kelch}$: when HtsRC is absent, loss of Kelch has no obvious consequence or additional phenotype.

HtsRC ring canal protein levels are dependent on Kelch

If HtsRC levels at ring canals are regulated by $CRL3^{Kelch}$-mediated ubiquitylation, partial loss-of-function mutations in *hts* may be suppressed by mutations in *kelch*. We reduced the germline

Development (2019) 146, dev169219. doi:10.1242/dev.169219

expression of HtsRC using an shRNA driven by *matGal4* (Yan et al., 2014) (Fig. 5A,B). When *hts* shRNA was expressed in a *kelch* mutant background, HtsRC levels at ring canals were increased compared with expression of *hts* shRNA in wild type (Fig. 5C).

We also tested whether HtsRC protein levels are dependent on Kelch. Using western analysis, we have been unable to detect a significant change in endogenous HtsRC levels in a Kelch-dependent manner. We suspect that this is because western analysis does not distinguish between the cytoplasmic pool of HtsRC and ring canal-localized HtsRC. To overcome this challenge, we used a transgenic GFP-tagged HtsRC construct driven by *matGal4* to assess HtsRC levels by GFP fluorescence (Fig. 5D,E) and western blotting (Fig. S5). Our goal was to increase our signal-to-noise ratio of ring canal-localized HtsRC by increasing its expression levels, so that any alteration of its levels by Kelch would be more easily detectable and quantifiable. HtsRC::GFP fluorescent protein levels were drastically reduced in egg chambers co-expressing mCherry::Kelch compared with mCherry control (Fig. 5D,E). Furthermore, western analysis revealed that total HtsRC protein species decreased significantly upon co-expression of mCherry::Kelch compared with mCherry control (Fig. S5). Of note, the levels of HtsRC::GFP species were most dramatically decreased upon Kelch overexpression, whereas endogenous HtsRC remained mostly unchanged (Fig. S5).

Finally, we examined the levels at ring canals of HtsRC::Venus fluorescent fusion protein expressed from a BAC transgene in the context of varying *kelch* gene copies (Fig. 5F,G). The pattern and levels of Venus fluorescence recapitulated localization patterns observed with the HtsRC monoclonal antibody. Furthermore, the expression of HtsRC::Venus was sufficient to rescue the loss of ring canal F-actin in *htsRC*-specific mutants, similar to *otu-ovhts::GFP* in Fig. S4. HtsRC::Venus fluorescent protein levels progressively increased as *kelch* gene copy number decreased (Fig. 5F). This effect was quantified by calculating the maximum fluorescence intensity of HtsRC::Venus for individual ring canals analyzed in four genotypes (Fig. 5G). The mean maximum fluorescence intensity of HtsRC::Venus progressively increased as *kelch* gene copy was reduced (compare black, green and blue data). These data show that Kelch protein levels directly affect ring canal-localized HtsRC protein levels.

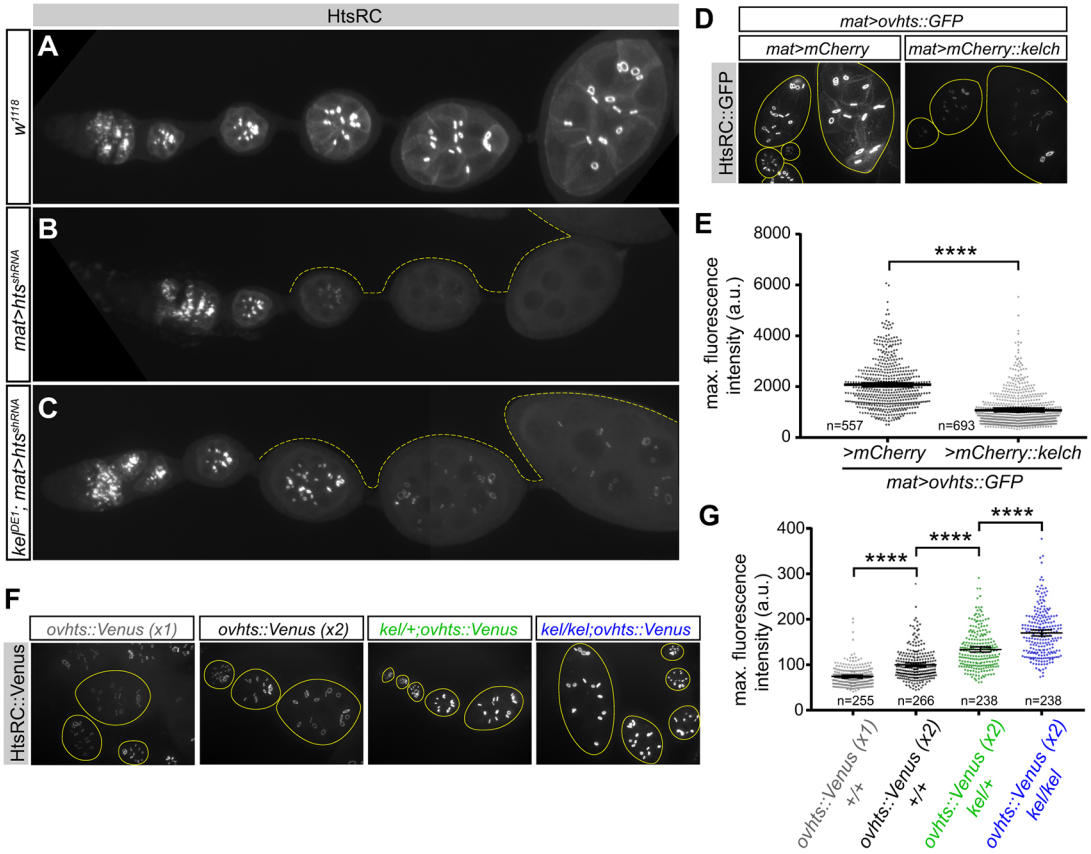

Fig. 5. HtsRC ring canal protein levels are dependent on Kelch. (A) Wild-type HtsRC expression in the germarium and subsequent stages. (B) *matGal4*-driven expression of a shRNA against *hts* resulted in near elimination of HtsRC from the germline in stages where *matGal4* expression was high (yellow dotted line indicates *matGal4* expression pattern). (C) Mutations in *kelch* suppressed the *hts* shRNA knockdown phenotype, resulting in detectable HtsRC in stage 2-8 egg chambers. The image is a mosaic created from two images using the MosaicJ plug-in from FIJI. (D) HtsRC::GFP fluorescent protein levels decreased with mCherry::Kelch co-expression compared with mCherry control expression. All constructs were driven by *matGal4*. Individual egg chambers are outlined in yellow. (E) Quantification of HtsRC::GFP fluorescent protein levels at ring canals. ****P<0.0001; Student's t-test. (F) HtsRC::Venus fluorescence levels at ring canals increased in a dose-dependent manner depending on *kelch* gene copy. Individual egg chambers are outlined in yellow. (G) Quantification of HtsRC::Venus fluorescent protein levels at ring canals. The mean maximum fluorescence intensity of the *ovhts::Venus x2* sample (black) was normalized to 100 relative fluorescence units. For E and G, data points in the scatter plot represent the maximum fluorescence intensity of HtsRC::Venus or HtsRC::GFP for each ring canal measured. Bars represent the maximum fluorescence intensity as mean±95% confidence interval of HtsRC::Venus or HtsRC::GFP. *n* denotes number of ring canals analyzed. ****P<0.0001; one-way ANOVA, Tukey's multiple comparison test. See also Fig. S5.

Development (2019) 146, dev169219. doi:10.1242/dev.169219

Removal of the Kelch NTR results in hyper-active Kelch

Kelch contains an N-terminal region (NTR) of 120 amino acids that is rich in low-complexity sequence (Fig. 6A). We previously analyzed a transgene encoding a Kelch protein lacking the NTR expressed at low levels throughout oogenesis using the *otu* promoter (Robinson and Cooley, 1997). *otu*-driven expression of Kelch$^{\Delta NTR}$ resulted in a dominant-negative, female-sterile phenotype due to the destabilization of germ cell membranes. This phenotype was attributed to the premature localization of Kelch$^{\Delta NTR}$ to ring canals (Robinson and Cooley, 1997). Given our results indicating that Kelch regulates HtsRC levels through the UPS, we re-examined the phenotype caused by Kelch$^{\Delta NTR}$ expression by creating a *UASp-kelch$^{\Delta NTR}$* transgene to express the Kelch$^{\Delta NTR}$ protein with greater control over the timing and level of expression. When we expressed wild-type Kelch at high levels using matGal4, the females were fertile with normal localization of HtsRC, consistent with our previous results (Fig. 6C; see also Fig. S5). In contrast, females expressing Kelch$^{\Delta NTR}$ were sterile, similar to previous results with *otu-kelch$^{\Delta NTR}$* constructs. HtsRC was nearly undetectable within the expression domain of matGal4 (Fig. 6D,D′), and *mat>kelch$^{\Delta NTR}$* egg chambers failed to complete oogenesis.

Expression of Kelch$^{\Delta NTR}$ at low levels using the weak *otu-Gal4::VP16* driver (*otuGal4*) resulted in a similar but less severe phenotype, and western blotting revealed reduced levels of HtsRC (Fig. 6E,F). When we compared the expression levels of Kelch$^{\Delta NTR}$ with wild-type Kelch driven by *otuGal4*, we found that Kelch$^{\Delta NTR}$ was expressed at much higher levels than wild-type Kelch (Fig. 6E,G), suggesting that loss of the NTR resulted in a stabilized protein. This raised the possibility that elevated CRL3^{Kelch} activity toward HtsRC may have resulted from the increased quantities of a stabilized Kelch$^{\Delta NTR}$. This would be similar to human mutations in KLHL24 that result in the production of a BBK protein that lacks its N-terminal region, leading to increased levels of KLHL24 and elevated levels of CRL3^{KLHL24} activity (Lin et al., 2016). To address the effect of differing levels of Kelch, we compared the effects of Kelch$^{\Delta NTR}$ driven by *otuGal4* with wild-type Kelch driven by *matGal4*. Wild-type Kelch driven by *matGal4* was present at twice the level of Kelch$^{\Delta NTR}$ driven by *otuGal4* (Fig. 6E,G); however, HtsRC levels were only reduced upon expression of Kelch$^{\Delta NTR}$. This suggests that altered regulation of Kelch$^{\Delta NTR}$, rather than increased quantity, is responsible for the apparent gain-of-function effects seen with Kelch$^{\Delta NTR}$ expression. Removal of the NTR appears to result in a hyper-active form of Kelch.

A PEAEQ sequence motif in HtsRC is necessary for its interaction with Kelch

Identification of the conserved PEAEQ sequence in HtsRC and other KREP-interacting proteins suggested this motif is a binding site for the Kelch KREP domain. If this is the case, and if HtsRC ubiquitylation is essential for ring canal cytoskeletal organization, then mutations in the *hts* PEAEQ motif that inhibit Kelch binding should result in a *kelch*-like phenotype. To test this, we used CRISPR/Cas9 NHEJ mutagenesis to create mutations in the PEAEQ sequence (Fig. 7A).

We recovered in-frame deletions of both E922 and Q925 in the PEAEQ motif, and in marked contrast to truncation mutations that lack a robust ring canal F-actin cytoskeleton (Fig. 4 and Fig. S4), the in-frame deletions resulted in phenotypes similar to *kelch* loss-of-function mutants. The stronger allele, a deletion of the E922 codon (*hts$^{\Delta E922}$*), resulted in a phenotype indistinguishable from the *kel^{DE1}* null allele (Fig. 7B-D): F-actin and the mutant HtsRC protein accumulated in ring canals, and the flies were sterile. The levels of

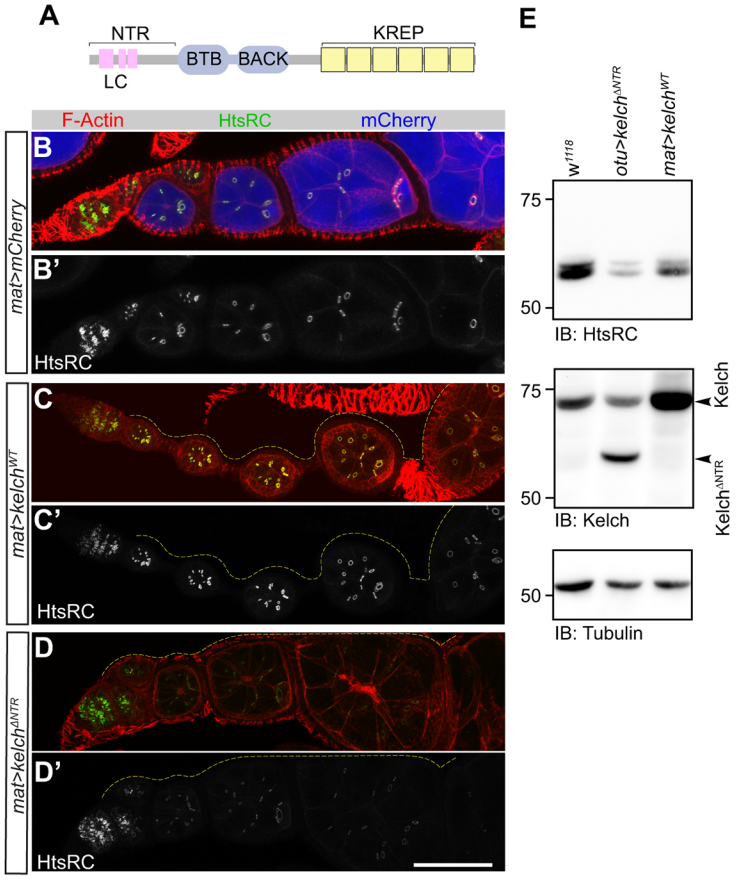

Fig. 6. Removal of the Kelch NTR results in hyper-active Kelch. (A) Cartoon of Kelch protein motifs, with low-complexity regions (LC) in the NTR (pink boxes). (B,B′) Control flies expressing mCherry under control of the *matGal4* driver revealed the expression domain of *matGal4* (blue) and had the wild-type pattern of HtsRC accumulation in young egg chambers. (C,C′) Expression of wild-type Kelch protein with the *matGal4* driver resulted in a normal distribution of HtsRC in egg chambers. (D,D′) *matGal4*-driven expression of Kelch$^{\Delta NTR}$ resulted in dramatic loss of HtsRC fluorescence compared with expression of wild-type Kelch. Yellow dotted line indicates the expression domain of *matGal4*; HtsRC levels in wild type and *matGal4>kelch$^{\Delta NTR}$* were comparable in the germarium, where the *matGal4* driver is not expressed. (E) Representative western blots showing levels of HtsRC and Kelch. A Tubulin immunoblot is shown as a loading control. (F) Expression of Kelch$^{\Delta NTR}$ driven by *otuGal4* resulted in reduced HtsRC protein compared with *w^{1118}* or *matGal4>kelch^{WT}*, despite higher levels of Kelch in *matGal4>kelch^{WT}* (see G). *P<0.05. (G) Kelch$^{\Delta NTR}$ driven by *otuGal4* resulted in approximately twice the level of endogenous Kelch. *matGal4*-driven expression of wild-type Kelch resulted in an approximately fivefold increase in Kelch expression.

Development (2019) 146, dev169219. doi:10.1242/dev.169219

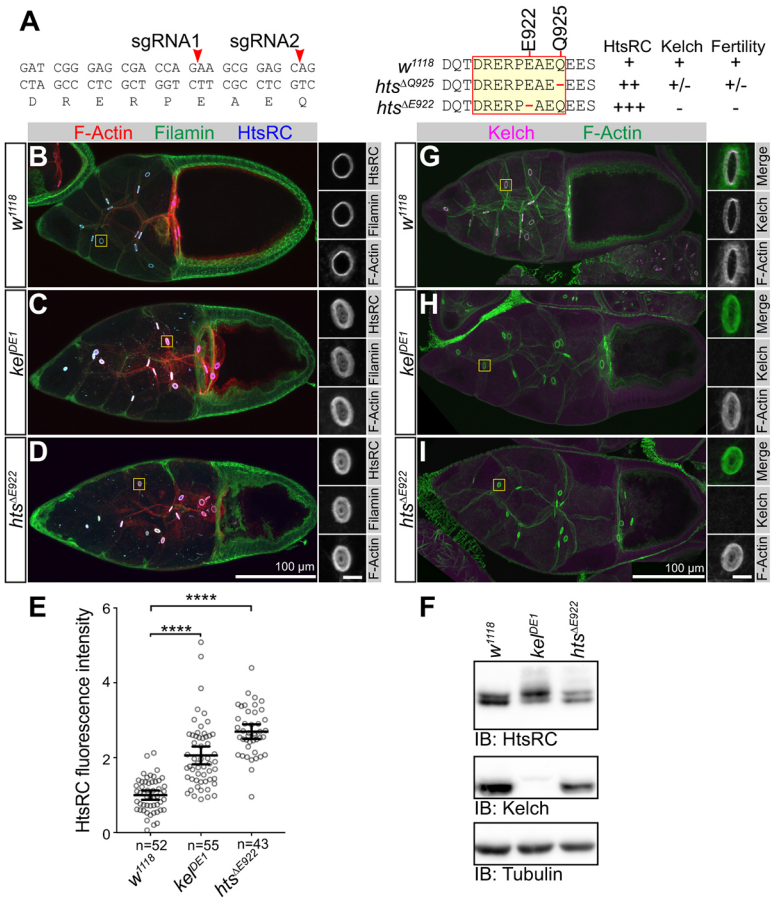

Fig. 7. A PEAEQ sequence motif in HtsRC is necessary for HtsRC interaction with Kelch. (A) Location of sgRNAs targeting the HtsRC PEAEQ motif (left) and summary of single-codon deletion mutations in PEAEQ sequence (middle). Red arrowheads indicate locations of sgRNA-directed Cas9-mediated cleavages. $hts^{\Delta E992}$ is an in-frame deletion resulting in a single amino acid deletion of the conserved E922 residue; $hts^{\Delta Q925}$ deletes Q925. Fertility and relative HtsRC and Kelch immunofluorescence levels at ring canals are summarized on the right. (B-D) Control (w^{1118}), $hts^{\Delta E992}$ and kel^{DE1} egg chambers labeled to reveal F-actin, HtsRC and Filamin. Homozygous $hts^{\Delta E992}$ egg chambers and ring canals were indistinguishable from kel^{DE1}. (E) Measured fluorescence intensity of HtsRC immunolabeled ring canals. Bars represent the fluorescence intensity as mean±95% confidence interval. ****P<0.0001; one-way ANOVA with Dunnett's multiple comparison test. (F-I) Kelch localization in control (w^{1118}), $hts^{\Delta E992}$ and kel^{DE1} egg chambers. Kelch localized to ring canals in wild-type egg chambers (G), but not in $hts^{\Delta E992}$ mutants (I), similar to *kelch* loss-of-function mutations (H), despite being expressed at normal levels (F). For B-D and G-I, ring anals within yellow box are shown in the inset to the right. Scale bar: 5 µm in inset. (F) Western blot showing steady-state levels of HtsRC and Kelch; Tubulin serves as a loading control. Overall HtsRC levels were not significantly increased compared with wild type. See also Fig. S6.

HtsRC at ring canals were twofold higher in $hts^{\Delta E922}$ and kel^{DE1} mutants compared with wild type (Fig. 7E). In addition, we found that, in $hts^{\Delta E922}$ mutants, Kelch no longer localized to ring canals (Fig. 7G-I), despite Kelch protein being present (Fig. 7F). Curiously, although increased levels of HtsRC at ring canals in *kelch* or *htsRC* PEAEQ mutants were obvious by immunofluorescence, we detected no difference in their steady-state accumulation by western blot (Fig. 7H). The $hts^{\Delta Q925}$ allele appeared to be weaker, and levels of HtsRC measured at ring canals were intermediate between wild type and $hts^{\Delta E922}$ mutants (Fig. S6A-C,G). Consistent with this result, Kelch was detected at $hts^{\Delta Q925}$ ring canals, but at reduced levels compared with wild type (Fig. S6D-F,H). Together, these results provide compelling *in vivo* evidence that the PEAEQ sequence is a binding site for Kelch.

DISCUSSION

In this study, we provide evidence that $CRL3^{Kelch}$ targets HtsRC at ring canals for ubiquitylation and proteasome-mediated destruction, providing a mechanism for how Kelch shapes the cytoskeleton during ring canal growth. Four lines of evidence support the idea that HtsRC is the key substrate of $CRL3^{Kelch}$: first, we detected HtsRC in a complex with the substrate-binding KREP domain of Kelch; second, we showed that HtsRC is ubiquitylated in cultured cells and in ovarian cells; third, we showed that levels of HtsRC are sensitive to the dose of Kelch; and, finally, we identified a putative binding motif in HtsRC that, when mutated, recapitulates the *kelch* phenotype and results in a loss of Kelch localization to ring canals. Together, these results provide strong evidence that HtsRC levels at ring canals are controlled by $CRL3^{Kelch}$-mediated targeted destruction to promote the coordinated expansion of the ring canal cytoskeleton. We were unable to demonstrate that all HtsRC ubiquitylation is Kelch dependent. It is therefore possible that $CRL3^{Kelch}$ removes HtsRC specifically from the ring canal lumen through a UPS-independent mechanism.

A striking feature of many proteins identified by mass spectrometry in complex with the KREP domain was the presence of a linear PEAEQ peptide motif. Two human BBK proteins, KLHL2 and KLHL3, are most closely related to *Drosophila* Kelch, and both have been shown to bind a similar EPEEPEADQ motif in WNK4, a substrate of KLHL3 (Schumacher et al., 2014). A structure of a KLHL3-WNK4 peptide complex revealed that the EPEEPEADQ peptide binds on the top surface of the KLHL3 KREP β-propeller, making extensive contacts with inter-strand surface loops derived from blades 2-4. We propose that the HtsRC PEAEQ motif binds *Drosophila* Kelch in a similar manner, and the prevalence of PEAEQ proteins we identified by both pulldown and yeast two-hybrid screening suggests that proteins with PEAEQ-like linear motifs are potential targets of Kelch and closely related BBK proteins.

In contrast, Keap1, a more distantly related BBK protein, targets its substrate Nrf2 for ubiquitylation through a high-affinity interaction with a short DxETGE sequence (Lo et al., 2006). A structure of the Keap1–DxETGE peptide complex revealed that Keap1 also engages its target peptide through contacts with surface loops extending from the top of the Keap1 β-propeller structure, similar to the KLHL3–PEADQ interaction. Unlike KLHL2 and KLHL3, however, the Nrf2 DxETGE peptide was found to be closely associated with surface loops derived from blades 1, 5 and 6; it therefore appears that the Keap1 KREP domain binds the DxETGE peptide in a manner distinct from the KLHL3-PEADQ

Development (2019) 146, dev169219. doi:10.1242/dev.169219

interaction. These observations suggest that subfamilies of BBK proteins engage substrates through distinct short peptide motifs. A more thorough understanding of BBK substrate interaction interfaces will be important for the development of pharmacological inhibitors or biological therapies, in order to target disease-relevant BBK proteins or their substrates.

Interactions between ubiquitin ligases and their substrates are typically regulated such that substrate ubiquitylation is restricted to the appropriate time and place. The Germ cell-less protein (GCL) is a component of a CRL3 that degrades the Torso receptor tyrosine kinase in order to maintain primordial germ cell fate (Pae et al., 2017). GCL is located at the nuclear envelope during interphase, and is only free to act following nuclear envelope breakdown during mitosis. Mutants that disrupt this mode of regulation result in the apparent ubiquitylation of inappropriate substrates and a severe germ cell defect (Pae et al., 2017). KLHL10, a BBK CRL3 substrate adaptor required for spermatid differentiation, is regulated by Scotti, a protein that acts as a pseudosubstrate inhibitor of $CRL3^{KLHL10}$ to regulate its activity in a graded fashion during spermatid elongation (Arama et al., 2007; Kaplan et al., 2010). We found that the Kelch NTR is important in regulating $CRL3^{Kelch}$ activity. We have previously observed that transgenic constructs driving low-level germline expression of $Kelch^{\Delta NTR}$ resulted in a dominant female-sterile phenotype (Robinson and Cooley, 1997). Our observation that $Kelch^{\Delta NTR}$ expression depletes HtsRC from germline cells suggests that $Kelch^{\Delta NTR}$ is a hyperactive protein that targets HtsRC in an unregulated manner. We note that the phenotype of $Kelch^{\Delta NTR}$ is similar to, but more severe than, loss-of-function mutations in *htsRC*, suggesting that the $Kelch^{\Delta NTR}$ may target proteins that are not normally substrates of $CRL3^{Kelch}$ during oogenesis.

The *Drosophila* Kelch NTR is a 120 amino acid extension rich in low-complexity sequence. It is conserved in Kelch orthologs in insects, but not in KLHL2 and KLHL3. However, 13 human BBK proteins have N-terminal extensions greater than 60 amino acids, and many of these are rich in low-complexity sequence. Interestingly, gain-of-function mutations in one of these genes, KLHL24, produce a mutant protein lacking part of its NTR that accumulates to high levels, resulting in unregulated ubiquitylation and degradation of its substrate, keratin 14, which causes skin fragility (Lin et al., 2016). Stabilization of mutant KLHL24 results from impaired auto-catalytic ubiquitylation and degradation of KLHL24, a commonly observed feature of CRLs (de Bie and Ciechanover, 2011). Although Kelch also undergoes Cul3-dependent autocatalytic degradation (Hudson and Cooley, 2010; Hudson et al., 2015), we do not think the hyperactive phenotype of $Kelch^{\Delta NTR}$ is simply a consequence of increased protein levels as elevated levels of wild-type Kelch do not have a similar phenotype.

Our results support a model in which $CRL3^{Kelch}$ targets HtsRC located at ring canals for ubiquitylation, leading to its degradation by the proteasome (Fig. 8). Consistent with this model, we found that, in cultured cells, HtsRC is stabilized upon proteasome inhibition, and that its stabilization is accompanied by the presence of high molecular weight ubiquitylated forms. In addition, we present direct evidence that HtsRC is ubiquitylated in ovarian extracts. We did not find HtsRC ubiquitylation was strictly dependent on Kelch, however; nor did we observe an increase in HtsRC levels by western blotting. It is possible that these discrepancies arise from the existence of two pools of HtsRC: an insoluble pool associated with the ring canal cytoskeleton; and a second, more soluble, cytoplasmic pool of HtsRC. We suspect that a distinct ubiquitylation pathway targets HtsRC in the cytosol and that the ubiquitylated HtsRC we observe in *kelch* mutants is a result of this alternative pathway. Our previous work supports the idea of a Kelch-independent degradation pathway acting on HtsRC present in the cytosol. HtsRC is selectively maintained in egg chambers; during the germline mitotic divisions in the germarium, both HtsF and HtsRC are produced, but only HtsF is observed whereas HtsRC appears to be actively degraded (Petrella et al., 2007). The degradation of HtsRC in the germline mitotic region is independent of Kelch, as HtsRC is also undetectable during mitosis in *kelch* mutants. HtsRC has also been suggested to function in other F-actin-rich structures in egg chambers, including nurse cell actin cables (Huelsmann et al., 2013) and the oocyte cortical cytoskeleton (Pokrywka et al., 2014). An alternative ubiquitylation pathway may regulate these non-ring canal functions of HtsRC. In addition, if cytoplasmic HtsRC is more easily extracted than the ring canal-associated HtsRC, it could mask differences in levels of the ring canal-HtsRC on western blots. Nevertheless, the findings that HtsRC is poly-ubiquitylated in ovaries and that its levels at the ring canal are regulated by Kelch strongly support a model for ring canal-specific HtsRC degradation mediated by $CRL3^{Kelch}$.

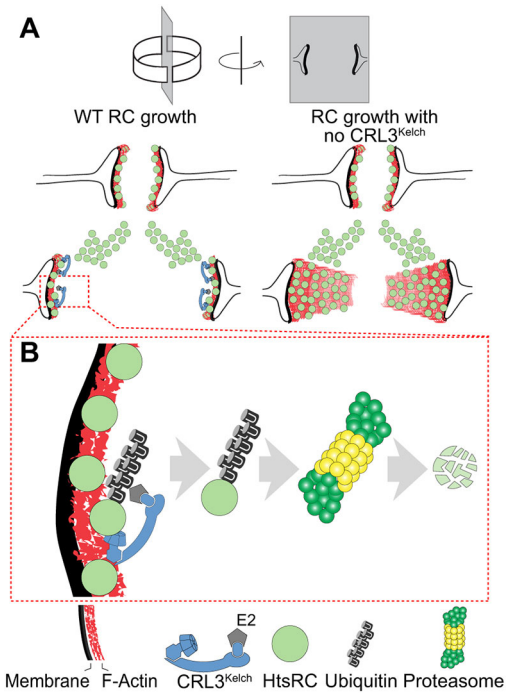

Fig. 8. Model for ring canal growth regulated by $CRL3^{Kelch}$. (A) Wild-type (WT) and *kelch* ring canals diagrammed in cross-section. Ring canals recruit HtsRC, which results in the accumulation of a robust F-actin cytoskeleton that supports ring canal growth. (B) In wild type, $CRL3^{Kelch}$ ubiquitylates HtsRC, targeting it for destruction by the proteasome. Removal of HtsRC by $CRL3^{Kelch}$-mediated destruction is required for the disassembly of the ring canal cytoskeleton from the ring canal lumen as the ring canal expands.

Based on our results, we propose that HtsRC is the key driver of ring canal growth (Fig. 8A). HtsRC is essential for the dynamic and robust F-actin cytoskeleton that lines the lumen of the ring canal; *hts* mutant egg chambers display multiple phenotypes, including the failure of F-actin to accumulate at ring canals (Petrella et al., 2007; Yue and Spradling, 1992), and our new exon 12 mutations affect only ring canals. The molecular mechanism by which HtsRC recruits F-actin to ring canals is not known; sequence analysis of HtsRC reveals no recognizable motifs aside from a predicted coiled-coil structure at its C terminus. One notable biochemical feature of HtsRC is its poor solubility. Ovarian lysates contain little soluble

Development (2019) 146, dev169219. doi:10.1242/dev.169219

HtsRC, and our attempts to produce soluble recombinant protein in its native state for *in vitro* studies have had limited success (J.A.G., unpublished). We speculate that the HtsRC at the ring canal may function by forming an insoluble matrix on which the dynamic ring canal F-actin cytoskeleton is assembled, driving the expansion of the ring canal diameter. However, to allow for the coordinated expansion of the ring canal lumen, HtsRC and associated proteins must be disassembled at the luminal surface, and this requires targeting by $CRL3^{Kelch}$ and the UPS. This represents an unusual mechanism for cytoskeletal remodeling, which generally relies on non-destructive mechanisms to create and dismantle cytoskeletal assemblies. However, removal by the UPS may be the only effective way to control the potent activity of HtsRC. Regulation of cytoskeletal structures by the ubiquitin-proteasome system is an emerging regulatory mechanism (Deng and Huang, 2014). However, most previous studies have used yeast or cultured cells (Wang et al., 2003; Chen et al., 2009; Razinia et al., 2011, 2013; Juanes and Piatti, 2016; Girouard et al., 2016; Wu et al., 2018). Our work is one of few examples to date detailing the mechanism by which the UPS organizes and remodels a cytoskeletal structure in a metazoan developmental model system.

MATERIALS AND METHODS

Experimental model and subject details

Drosophila genetics

Drosophila were maintained at 25°C on standard fly food medium. Prior to ovary dissections, females were fattened on wet yeast paste overnight at 25°C. See Table S2 for a detailed list of fly stocks used in this study.

S2 cell culture

Drosophila S2 cells (DGRC) were cultured at 27°C in Schneider's *Drosophila* Media (Gibco) supplemented with 10% fetal bovine serum and 1× antibiotic-antimycotic (Gibco). We confirmed that the cells were not contaminated.

Affinity purification and mass spectrometry

The *cher*^{1} allele (89E) was recombined with the *UASp-TAPmCherry* (Neelakanta et al., 2012) and *UASp-TAPmCherry::KREP* (Hudson and Cooley, 2010) constructs integrated at the attP2 site (68A4), and also recombined with *matGal4::VP16* (mapped to 91D4 by inverse PCR). Recombinant chromosomes were balanced with a *TM3, hs-hid* balancer (Bloomington #1558) to allow for heat-shock-induced selection of desired cross progeny. Approximately 500 ovaries from *cher*^{1} mutant females expressing either TAPmCherry or TAPmCherry::KREP were homogenized in SBP lysis buffer [50 mM HEPES (pH 7.5), 150 mM NaCl, 2 mM EDTA, 0.5%Triton X-100, 10% glycerol, 1 mM PMSF and 5 µg/ml each of chymostatin, leupeptin, antipain and pepstatin] in a glass Duall homogenizer with a teflon pestle driven by motorized spinning. Lysates were clarified by centrifugation for 30 min at 20,000 ***g*** at 4°C, and approximately 40 mg of clarified supernatants were incubated with 75 µl streptavidin beads (Thermo Fisher Scientific, 53114). Beads were washed 2× in SBP lysis buffer followed by two additional washes in His-tag buffer [50 mM NaPi (pH 8), 300 mM NaCl, 5 mM imidazole, 0.2% Triton X-100]. Proteins bound to streptavidin beads were eluted in 1 ml 10 mM biotin in His-tag buffer for 20 min at 4°C. Eluted proteins were incubated with 75 µl 50% Ni^{++}-NTA slurry for 2 h, washed three times in His-tag buffer, and eluted twice in 35 µl SDS-PAGE sample buffer containing 200 mM DTT and 200 mM imidazole. Each sample (25 µl) was loaded on a 4-12% gradient NuPAGE gel and stained with EZBlue colloidal Coomassie (Sigma-Aldrich). A second 25 µl aliquot was analyzed at MS Bioworks by running the samples on a 10% Bis-Tris NuPAGE gel, slicing each lane into 10 equal fragments, and subjecting each fragment to in-gel trypsin digestion followed by LC-MS/MS on a Thermo Fisher Q Exactive instrument. Mass spectrometry data were searched against the Uniprot *Drosophila* proteome at MS Bioworks using Mascot (Matrix Science) and the results were parsed into Scaffold (Proteome Software) for further analysis.

Plasmids

To make pAHW-HtsRC::HA for expression of HtsRC in S2 cells, exon 12 of *ovhts* with a C-terminal 1xHA tag was PCR amplified to contain flanking attB1 and attB2 sites. The PCR product was recombined into the Gateway Donor vector pDONR201 in a Gateway BP Clonase II reaction (Thermo Fisher Scientific). The entry clone was further recombined into the Gateway Expression vector pAHW (*Drosophila* Gateway Vector Collection; *Drosophila* Genomics Resource Center, 1095) in an LR Clonase II reaction (Thermo Fisher Scientific). The resulting pAHW-HtsRC::HA expression plasmid allows for expression of HtsRC with a 3xHA N-terminal tag and 1xHA C-terminal tag, driven by the *Actin5C* promoter. *pUASp-kelch*$^{\Delta NTR}$ was generated by amplifying a region of the *kelch* CDS encoding amino acids Q121-M689, the same range used in earlier $Kelch^{\Delta NTR}$ constructs (Robinson and Cooley, 1997). PCR primers included flanking attB1 and attB2 Gateway recombination sites and the product was recombined first into pDONR201 and then into pPW-attB (a gift from Mike Buszczak, UT Southwestern Medical Center, TX, USA), an untagged UASp vector from the *Drosophila* Gateway collection modified to include a phiC-31 attB recombination target. The *pUASp-kelch*$^{\Delta NTR}$ was injected into a strain carrying the *attP2* phiC-31 landing site on Chromosome 3L at Rainbow transgenics. To construct *pUASp-7xHis::Ubiquitin*, a human HA-tagged ubiquitin cDNA was excised as an *Eco*RI-*Xho*I fragment from *pUASt-HA::Ubiquitin* (a gift from Tian Xu, Westlake University, China) and cloned into pBluescript II (Stratagene). The HA tag in this plasmid was replaced with oligonucleotides encoding a 7xHis tag by ligation into the *Nco*I and *Bgl*II sites, and the 7xHis::Ubiquitin fragment was then transferred to pMTV5 His (Invitrogen) as an *Eco*RI-*Xho*I fragment. 7xHis Ubiquitin from the pMTV5 plasmid was then cloned into pUASp as a *Kpn*I-*Xba* fragment. The plasmid was transformed into the w^{1118} strain using standard procedures.

Yeast two-hybrid screen

A cDNA encoding the Kelch KREP domain was cloned into pEG202, the bait vector for the LexA yeast two-hybrid system (Golemis et al., 2011). For the interaction screen, 6×10^{6} yeast transformants from the Ovo II ovarian 2-Hybrid cDNA library (Grosshans et al., 1999) were screened for interaction by β-galactosidase production on X-gal plates and by complementation of *leu2* auxotrophy. Two-hundred of the fastest growing colonies were selected for further analysis.

CRISPR/Cas9 mutagenesis of *hts*

Oligos encoding sgRNAs described in Table S2 were cloned into the *Bbs*I site of the *pBFvU6.2* vector (Kondo and Ueda, 2013) and integrated at the *attP2* or *attP40* phiC31 integration site (Groth et al., 2004). Mutagenesis was carried out in males expressing Cas9 from a germline promoter (*nanos-Cas9*; Port et al., 2014; Bloomington, 54591) in combination with ubiquitous sgRNA expression from the *snRNA:U6:96Ab* promoter. Single male progeny bearing CRISPR-mutagenized chromosomes were crossed to a deficiency for *hts* [*Df(2R)BSC135/CyO*, Bloomington, 9423], and hemizygous progeny were screened by sequencing and/or fertility tests. Balanced stocks were established for mutations of interest.

Construction of *TagRFP-T::ovhts::Venus* BAC transgene

BAC clone CH321-84O22 (Venken et al., 2009), which contains all of the *hts* locus on a 91 kb genomic fragment (chr2R:19,368,835…19,460,115, FlyBase release 6), was used as a template to introduce fluorescent protein-coding sequences. HA::Venus::FLAG sequence was inserted before the stop codon of exon 12, the exon encoding HtsRC (codon starting position chr2R:19,3399,860), using 2-step BAC recombineering. Briefly, a *RpsL-neo* selection cassette (Wang et al., 2009) was inserted using Kanamycin selection, and the *RpsL-neo* cassette was subsequently replaced with HA::Venus::FLAG using streptomycin counterselection. The same approach was then used to insert HA::TagRFP-T::FLAG before the first codon of *ovhts* exon 8 (Trp 473 of Ovhts polypeptide, codon starting position chr2R:19,409,361). Two additional rounds of recombineering were used to reduce the size of the BAC; the trimmed BAC contained a 44 kb genomic fragment from chr2R:19,390,835 (in *CG11257*) to chr2R:19,434,833 (in *Fak*). The BAC was injected into the *attP2* landing

Development (2019) 146, dev169219. doi:10.1242/dev.169219

site on chr3L at GenetiVision. TagRFP-T fluorescence was not observed in transformed lines, suggesting that the introduction of TagRFP-T into the Adducin portion of Ovhts was detrimental to its folding. However, Venus fluorescence recapitulated the expression and localization patterns that are observed with the HtsRC monoclonal antibody, indicating that the cleaved ring canal protein tagged with Venus was produced normally. Consistent with this, the HtsRC protein produced by this construct was sufficient to rescue the loss of ring canal F-actin in *htsRC*-specific mutants, similar to *otu-ovhts::GFP* in Fig. S4.

Fixation, immunofluorescence and imaging

Ovaries were fixed in 4% paraformaldehyde (Electron Microscopy Sciences) in PBS with or without 0.1% Triton X-100 for 10 min, washed in PBT (PBS, 0.1% Triton X-100, 0.5% BSA) and incubated in primary antibody in PBT at 4°C overnight. Antibodies and other fluorescent reagents are listed in Table S2. Samples were washed four times in PBT, and incubated with secondary antibodies and fluorescent phalloidin (if used) in PBT for 2 h at room temperature. Following secondary antibody incubation, samples were washed four times in PBT and mounted on slides in ProLong Gold or Diamond antifade reagents (Thermo Fisher Scientific). Samples were imaged on one of three microscopes: a Leica SP8 scanning confocal system using a 40× Plan Apo 1.30 NA objective; a Nikon TiE inverted microscope with a Yokogawa CSU-W1 spinning disc system, an Andor iXon Ultra888 1024×1024 EMCCD and 40× Plan Fluor 1.30 oil immersion objective; or a Zeiss Axiovert 200m inverted microscope with a CrEST X-light spinning disc system, Photometrics CoolSNAP HQ2 camera and either a 20× Plan Apo 0.8 NA objective or a 40× C-Apo 1.2 NA water-immersion objective. Images were processed and analyzed with ImageJ/FIJI or Imaris 9.0 (Bitplane).

Analysis of HtsRC ubiquitylation and stability in S2 cells

S2 cells at 50-80% confluency were transfected with 1 µg of pAHW-HtsRC::HA DNA following the Effectene Transfection Reagent protocol (Qiagen). To assess HtsRC ubiquitylation and stability in response to drug/inhibitor treatments, cells were treated with DMSO control (Sigma-Aldrich), 1 µM bortezomib (Cell Signaling) and/or 100 µg/ml cycloheximide (Sigma-Aldrich) beginning at 24 or 36 h post-transfection, as indicated in Fig. 2 legend. Cells were harvested at the indicated time points (0, 3 and 6 h following inhibitor treatment), lysed in SDS-PAGE sample buffer and analyzed by western analysis to visualize HtsRC and Tubulin protein levels. HtsRC protein levels were quantified using ImageJ by measuring the integrated density of HtsRC protein bands relative to Tubulin protein bands to control for protein loading. GraphPad Prism was used to perform a Student's *t*-test using data from three independent experiments.

Analysis of HtsRC ubiquitylation in ovaries

For His::Ubiquitin purifications, flies of genotype *UASp-7xHis::Ub/+; oskGal4/+; UASp-7xHis::Ub/shRNA-Rpn9*^{HMS01007} were used. For purifications in a *kelch* mutant background, flies of genotype *UASp-7xHis::Ub/+; kel*^{DE1}*, oskGal4/ kel*^{DE1}*; UASp-7xHis::Ub/shRNA-Rpn9*^{HMS01007} were used. Control purifications were performed using w^{1118}. Isolation of ubiquitylated proteins was based on established procedures (Laney and Hochstrasser, 2002). Briefly, ovaries from ∼200 flies of each genotype were lysed in a glass Duall homogenizer in His/Guanidine buffer: 6 M guanidine, 50 mM NaPi/10 mM Tris (pH 8), 300 mM NaCl, 20 mM imidazole, 0.1% Triton X-100, 10 mM *N*-ethylmaleimide, 1 mM PMSF and 5 µg/ml each of chymostatin, leupeptin, antipain and pepstatin. Lysates were clarified by centrifugation for 30 min at 20,000 ***g*** at 4°C and supernatants were incubated with 50 µl Ni^{++}-NTA resin (Qiagen) in His/Guanidine buffer for 4 h at 4°C. Beads were washed twice in His/Guanidine buffer, once in Urea wash buffer at pH 8 [8 M Urea, 50 mM NaPi/10 mM Tris (pH 8), 300 mM NaCl, 20 mM imidazole, 0.1% Triton X-100] and twice in Urea wash buffer (pH 6.0). Proteins were eluted in SDS-PAGE sample buffer containing 200 mM DTT and 200 mM imidazole and analyzed by immunoblotting.

Quantification of HtsRC immunolabeling at ring canals

Egg chambers were labeled with HtsRC 6A (Robinson et al., 1994) or Kel 1B monoclonal antibodies, both of which result in specific labeling of ring canals with little plasma membrane signal. Image stacks of wild-type and mutant egg chambers that included all ring canals in selected stage 10 egg chambers were collected on a spinning disc confocal with constant settings for exposure time, illumination power and camera gain. Image stacks were analyzed in Imaris using automatic 3D thresholding of HtsRC or Kelch signal to identify ring canal volumes, and the summed fluorescence intensity was calculated for each ring canal. Raw fluorescent intensities were normalized to the mean fluorescence intensity of the control sample, which was defined as 1.

Quantification of ring canal F-actin thickness

To measure ring canal F-actin thickness, egg chambers were stained with fluorescent phalloidin. Maximum intensity projections of imaged egg chambers were rendered using ImageJ, and ring canals that provided a full longitudinal cross-section with a top-down view were analyzed (see top panel of Fig. 3 for representative ring canals). A line was drawn through the center of measurable ring canals, and a F-actin fluorescence intensity plot spanning the line was generated. The full width at half maximum (FWHM) function of F-actin fluorescence intensity was calculated and used to approximate the thickness of the ring canal F-actin (see Hudson et al., 2015 for more details). Ring canals from stage 6 egg chambers were analyzed for Fig. 3A because that was the oldest stage the egg chambers progress to before undergoing degeneration (Hudson et al., 2015). For Fig. 3B, we analyzed ring canals from stage 9 egg chambers because those egg chambers were abundant, easily identifiable and the ring canals were larger, which was more advantageous for quantifying the F-actin thickness. For Fig. 3 graphs, *n* refers to the number of ring canals analyzed, the black line denotes the mean F-actin thickness, and error bars represent the 95% confidence interval. One-way ANOVA with Tukey's multiple comparison correction was used in GraphPad Prism to detect for statistically significant differences in the mean ring canal F-actin thickness between samples.

Quantification of HtsRC fluorescent fusion protein levels

To quantify how HtsRC fluorescent fusion protein levels were dependent on Kelch (Fig. 5), egg chambers of all stages were imaged on a Zeiss spinning disc microscope using the same exposure time (500 ms). Maximum intensity projections of imaged egg chambers were rendered in ImageJ, and the maximum fluorescence value for each ring canal was calculated. The mean maximum fluorescence intensity of *ovhts::Venus x2* sample (Fig. 5B, black) was normalized to 100 relative fluorescence units. Each plotted point represents the maximum fluorescence intensity of the HtsRC fluorescent fusion protein (HtsRC::Venus for Fig. 5B, HtsRC::GFP for Fig. 5D). *n* equals the number of ring canals analyzed and the black line represents the mean maximum fluorescence intensity while error bars represent 95% confidence interval. Statistical analyses (one-way ANOVA for Fig. 5B and Student's *t*-test for Fig. 5D) were performed in GraphPad Prism to test for differences in the average maximum fluorescence intensity between the various genotypes, as indicated in the figure legends. Data are compiled from two independent experiments.

Western analysis of HtsRC protein levels from ovary extracts

To analyze HtsRC protein levels by western analysis, ovary lysates were generated by homogenizing dissected ovaries in SDS-PAGE sample buffer. One ovary equivalent was loaded per lane and separated on a 8.5 or 9% polyacrylamide gel. Proteins were transferred to nitrocellulose membrane, stained with amido black to visualize total protein, blocked in 5% milk in TBST (Tris-buffered saline with 0.1% Tween-20) and probed with the following antibodies: anti-HtsRC, anti-Kelch and anti-Tubulin. Blots were incubated with HRP-conjugated secondary antibodies followed by ECL development (Bio-Rad) and imaged on a CCD camera (Protein Simple). For Fig. 6, levels of HtsRC, Kelch and β-Tubulin were measured using FIJI/ImageJ, with β-Tubulin serving as a loading control. Levels of HtsRC and Kelch are expressed relative to wild-type levels in w^{1118}, defined as 1. Data are from four independent experiments. For Fig. S5, total HtsRC protein levels were quantified using ImageJ by measuring the integrated density of HtsRC::GFP and HtsRC protein bands relative to amido black integrated density to control for protein levels loaded. HtsRC levels for mCherry-expressing control lysates were normalized to 1. HtsRC and HtsRC::GFP

levels were parsed apart for graphical visualization. Error bars represent s.e.m. Student's *t*-test was performed using GraphPad Prism. Data are from three independent experiments.

Quantification and statistical analysis

Data visualization and statistical analysis was performed in Prism (GraphPad). For quantification of protein levels by western blotting, error bars represent the mean±s.e.m. For all other quantification experiments, individual data points are plotted and the error bars represent the mean±95% confidence interval (CI), as indicated in the figure legend. Binomial test for enrichment of PEAEQ-containing proteins compared observed (15 PEAEQ proteins out of 141 KREP-interacting proteins) to expected [~3/141, based on the *Drosophila* genome encoding 262 PEAEQ proteins from 13,931 protein coding genes (Table S1)]. Other statistical tests used (one-way ANOVA or Student's *t*-test), *P* values and *n* are also listed in the figure legends.

Acknowledgements

We thank Jovan Williams and Sowjanya Kallakuri for their help in recombineering the Ovhts BAC transgene. We thank Tian Xu for providing access to the Leica SP8 confocal microscope. Stocks obtained from the Bloomington Drosophila Stock Center (NIH P40OD018537) were used in this study. We thank the TRiP at Harvard Medical School for providing transgenic RNAi fly stocks used in this study. We thank the Drosophila Genomics Resource Center, supported by NIH grant 2P40OD010949, for the S2 cells used in this study. J.A.G. was funded in part by a Gruber Science Fellowship from Yale University.

Competing interests

The authors declare no competing or financial interests.

Author contributions

Conceptualization: A.M.H., L.C.; Methodology: A.M.H., K.M.M., J.A.G., M.C.K., L.C.; Investigation: A.M.H., K.M.M., J.A.G., M.C.K.; Resources: A.M.H., K.M.M., M.C.K.; Data curation: A.M.H.; Writing - original draft: A.M.H., K.M.M.; Writing - review & editing: A.M.H., K.M.M., L.C.; Project administration: L.C.; Funding acquisition: L.C.

Funding

This work was supported by the National Institutes of Health (R01 GM043301 and RC1 GM091791 to L.C.). Partial support for predoctoral trainees was provided by National Institutes of Health training grants (T32 GM007223 for K.M.M., T32 GM007499 for J.A.G.]. Deposited in PMC for release after 12 months.

Supplementary information

Supplementary information available online at
http://dev.biologists.org/lookup/doi/10.1242/dev.169219.supplemental

References

Adams, J., Kelso, R. and Cooley, L. (2000). The kelch repeat superfamily of proteins: propellers of cell function. *Trends Cell Biol.* **10**, 17-24.

Arama, E., Bader, M., Rieckhof, G. E. and Steller, H. (2007). A ubiquitin ligase complex regulates caspase activation during sperm differentiation in Drosophila. *PLoS Biol.* **5**, e251.

Bastock, R. and St Johnston, D. (2008). Drosophila oogenesis. *Curr. Biol.* **18**, R1082-7.

Bomont, P., Cavalier, L., Blondeau, F., Ben Hamida, C., Belal, S., Tazir, M., Demir, E., Topaloglu, H., Korinthenberg, R., Tüysüz, B. et al. (2000). The gene encoding gigaxonin, a new member of the cytoskeletal BTB/kelch repeat family, is mutated in giant axonal neuropathy. *Nat. Genet.* **26**, 370-374.

Boyden, L. M., Choi, M., Choate, K. A., Nelson-Williams, C. J., Farhi, A., Toka, H. R., Tikhonova, I. R., Bjornson, R., Mane, S. M., Colussi, G. et al. (2012). Mutations in kelch-like 3 and cullin 3 cause hypertension and electrolyte abnormalities. *Nature* **482**, 98-102.

Chen, Y., Yang, Z., Meng, M., Zhao, Y., Dong, N., Yan, H., Liu, L., Ding, M., Peng, H. B. and Shao, F. (2009). Cullin mediates degradation of RhoA through evolutionarily conserved BTB adaptors to control actin cytoskeleton structure and cell movement. *Mol. Cell* **35**, 841-855.

de Bie, P. and Ciechanover, A. (2011). Ubiquitination of E3 ligases: self-regulation of the ubiquitin system via proteolytic and non-proteolytic mechanisms. *Cell Death Differ.* **18**, 1393-1402.

Deng, S. and Huang, C. (2014). E3 ubiquitin ligases in regulating stress fiber, lamellipodium, and focal adhesion dynamics. *Cell Adh. Migr.* **8**, 49-54.

Dhanoa, B. S., Cogliati, T., Satish, A. G., Bruford, E. A. and Friedman, J. S. (2013). Update on the Kelch-like (KLHL) gene family. *Hum. Genomics* **7**, 13.

Girouard, M.-P., Pool, M., Alchini, R., Rambaldi, I. and Fournier, A. E. (2016). RhoA proteolysis regulates the actin cytoskeleton in response to oxidative stress. *PLoS ONE* **11**, e0168641.

Golemis, E. A., Serebriiskii, I., Finley, R. L., Kolonin, M. G., Gyuris, J. and Brent, R. (2001). Interaction trap/two-hybrid system to identify interacting proteins. *Curr. Protoc. Cell Biol.* **8**, 17.3.1-17.3.42.

Grosshans, J., Schnorrer, F. and Nüsslein-Volhard, C. (1999). Oligomerisation of Tube and Pelle leads to nuclear localisation of dorsal. *Mech. Dev.* **81**, 127-138.

Groth, A. C., Fish, M., Nusse, R. and Calos, M. P. (2004). Construction of transgenic Drosophila by using the site-specific integrase from phage phiC31. *Genetics* **166**, 1775-1782.

Gupta, V. A. and Beggs, A. H. (2014). Kelch proteins: emerging roles in skeletal muscle development and diseases. *Skelet. Muscle* **4**, 11.

Haglund, K., Nezis, I. P. and Stenmark, H. (2011). Structure and functions of stable intercellular bridges formed by incomplete cytokinesis during development. *Commun. Integr. Biol.* **4**, 1-9.

Hudson, A. M. and Cooley, L. (2010). Drosophila Kelch functions with Cullin-3 to organize the ring canal actin cytoskeleton. *J. Cell Biol.* **188**, 29-37.

Hudson, A. M., Mannix, K. M. and Cooley, L. (2015). Actin cytoskeletal organization in drosophila germline ring canals depends on Kelch function in a Cullin-RING E3 ligase. *Genetics* **201**, 1117-1131.

Huelsmann, S., Ylänne, J. and Brown, N. (2013). Filopodia-like actin cables position nuclei in association with perinuclear actin in Drosophila nurse cells. *Dev. Cell* **26**, 604-615.

Juanes, M. A. and Piatti, S. (2016). Control of formin distribution and actin cable assembly by the E3 ubiquitin ligases Dma1 and Dma2. *Genetics* **204**, 205-220.

Kaplan, Y., Gibbs-Bar, L., Kalifa, Y., Feinstein-Rotkopf, Y. and Arama, E. (2010). Gradients of a ubiquitin E3 ligase inhibitor and a caspase inhibitor determine differentiation or death in spermatids. *Dev. Cell* **19**, 160-173.

Komander, D. and Rape, M. (2012). The ubiquitin code. *Annu. Rev. Biochem.* **81**, 203-229.

Kondo, S. and Ueda, R. (2013). Highly improved gene targeting by germline-specific Cas9 expression in Drosophila. *Genetics* **195**, 715-721.

Laney, J. D. and Hochstrasser, M. (2002). Assaying protein ubiquitination in Saccharomyces cerevisiae. *Meth. Enzymol.* **351**, 248-257.

Li, X., Zhang, D., Hannink, M. and Beamer, L. J. (2004). Crystal structure of the Kelch domain of human Keap1. *J. Biol. Chem.* **279**, 54750-54758.

Li, W., Bengtson, M. H., Ulbrich, A., Matsuda, A., Reddy, V. A., Orth, A., Chanda, S. K., Batalov, S. and Joazeiro, C. A. P. (2008). Genome-wide and functional annotation of human E3 ubiquitin ligases identifies MULAN, a mitochondrial E3 that regulates the organelle's dynamics and signaling. *PLoS ONE* **3**, e1487.

Lin, Z., Li, S., Feng, C., Yang, S., Wang, H., Ma, D., Zhang, J., Gou, M., Bu, D., Zhang, T. et al. (2016). Stabilizing mutations of KLHL24 ubiquitin ligase cause loss of keratin 14 and human skin fragility. *Nat. Genet.* **48**, 1508-1516.

Lo, S. C., Li, X., Henzl, M. T., Beamer, L. J. and Hannink, M. (2006). Structure of the Keap1:Nrf2 interface provides mechanistic insight into Nrf2 signaling. *EMBO J.* **25**, 3605-3617.

Neelakanta, G., Hudson, A. M., Sultana, H., Cooley, L. and Fikrig, E. (2012). Expression of Ixodes scapularis antifreeze glycoprotein enhances cold tolerance in Drosophila melanogaster. *PLoS ONE* **7**, e33447.

Padmanabhan, B., Tong, K. I., Ohta, T., Nakamura, Y., Scharlock, M., Ohtsuji, M., Kang, M.-I., Kobayashi, A., Yokoyama, S. and Yamamoto, M. (2006). Structural basis for defects of Keap1 activity provoked by its point mutations in lung cancer. *Mol. Cell* **21**, 689-700.

Pae, J., Cinalli, R. M., Marzio, A., Pagano, M. and Lehmann, R. (2017). GCL and CUL3 control the switch between cell lineages by mediating localized degradation of an RTK. *Dev. Cell* **42**, 130-142.e7.

Petrella, L. N., Smith-Leiker, T. and Cooley, L. (2007). The Ovhts polyprotein is cleaved to produce fusome and ring canal proteins required for Drosophila oogenesis. *Development* **134**, 703-712.

Pokrywka, N. J., Zhang, H. and Raley-Susman, K. (2014). Distinct roles for hu li tai shao and swallow in cytoskeletal organization during Drosophila oogenesis. *Dev. Dyn.* **243**, 906-916.

Port, F., Chen, H.-M., Lee, T. and Bullock, S. L. (2014). Optimized CRISPR/Cas tools for efficient germline and somatic genome engineering in Drosophila. *Proc. Natl. Acad. Sci. USA* **111**, E2967-E2976.

Prag, S. and Adams, J. C. (2003). Molecular phylogeny of the kelch-repeat superfamily reveals an expansion of BTB/kelch proteins in animals. *BMC Bioinformatics* **4**, 42.

Razinia, Z., Baldassarre, M., Bouaouina, M., Lamsoul, I., Lutz, P. G. and Calderwood, D. A. (2011). The E3 ubiquitin ligase specificity subunit ASB2alpha targets filamins for proteasomal degradation by interacting with the filamin actin-binding domain. *J. Cell Sci.* **124**, 2631-2641.

Razinia, Z., Baldassarre, M., Cantelli, G. and Calderwood, D. A. (2013). ASB2α, an E3 ubiquitin ligase specificity subunit, regulates cell spreading and triggers proteasomal degradation of filamins by targeting the filamin calponin homology 1 domain. *J. Biol. Chem.* **288**, 32093-32105.

Robinson, D. N. and Cooley, L. (1997). Drosophila kelch is an oligomeric ring canal actin organizer. *J. Cell Biol.* **138**, 799-810.

Development (2019) 146, dev169219. doi:10.1242/dev.169219

Robinson, D. N., Cant, K. and Cooley, L. (1994). Morphogenesis of Drosophila ovarian ring canals. *Development* **120**, 2015-2025.

Robinson, D. N., Smith-Leiker, T. A., Sokol, N. S., Hudson, A. M. and Cooley, L. (1997). Formation of the Drosophila ovarian ring canal inner rim depends on *cheerio*. *Genetics* **145**, 1063-1072.

Schumacher, F.-R., Sorrell, F. J., Alessi, D. R., Bullock, A. N. and Kurz, T. (2014). Structural and biochemical characterization of the KLHL3-WNK kinase interaction important in blood pressure regulation. *Biochem. J.* **460**, 237-246.

Shibata, S., Zhang, J., Puthumana, J., Stone, K. L. and Lifton, R. P. (2013). Kelch-like 3 and Cullin 3 regulate electrolyte homeostasis via ubiquitination and degradation of WNK4. *Proc. Natl. Acad. Sci. USA* **110**, 7838-7843.

Sokol, N. S. and Cooley, L. (1999). Drosophila filamin encoded by the cheerio locus is a component of ovarian ring canals. *Curr. Biol.* **9**, 1221-1230.

Venken, K. J. T., Carlson, J. W., Schulze, K. L., Pan, H., He, Y., Spokony, R., Wan, K. H., Koriabine, M., de Jong, P. J., White, K. P. et al. (2009). Versatile P[acman] BAC libraries for transgenesis studies in *Drosophila melanogaster*. *Nat. Methods* **6**, 431-434.

Wang, H.-R., Zhang, Y., Ozdamar, B., Ogunjimi, A. A., Alexandrova, E., Thomsen, G. H. and Wrana, J. L. (2003). Regulation of cell polarity and protrusion formation by targeting RhoA for degradation. *Science* **302**, 1775-1779.

Wang, S., Zhao, Y., Leiby, M. and Zhu, J. (2009). A new positive/negative selection scheme for precise BAC recombineering. *Mol. Biotechnol.* **42**, 110-116.

Waterhouse, A. M., Procter, J. B., Martin, D. M., Clamp, M. and Barton, G. J. (2009). Jalview Version 2–a multiple sequence alignment editor and analysis workbench. *Bioinformatics* **25**, 1189-1191.

Wu, B., Yang, S., Sun, H., Sun, T., Ji, F., Wang, Y., Xu, L. and Zhou, D. (2018). Keap1 inhibits metastatic properties of NSCLC cells by stabilizing architectures of F-actin and focal adhesions. *Mol. Cancer Res.* **16**, 508-516.

Xu, L., Wei, Y., Reboul, J., Vaglio, P., Shin, T.-H., Vidal, M., Elledge, S. J. and Harper, J. W. (2003). BTB proteins are substrate-specific adaptors in an SCF-like modular ubiquitin ligase containing CUL-3. *Nature* **425**, 316-321.

Xue, F. and Cooley, L. (1993). kelch encodes a component of intercellular bridges in Drosophila egg chambers. *Cell* **72**, 681-693.

Yan, D., Neumüller, R. A., Buckner, M., Ayers, K., Li, H., Hu, Y., Yang-Zhou, D., Pan, L., Wang, X., Kelley, C. et al. (2014). A regulatory network of Drosophila germline stem cell self-renewal. *Dev. Cell* **28**, 459-473.

Yatsenko, A. N., Roy, A., Chen, R., Ma, L., Murthy, L. J., Yan, W., Lamb, D. J. and Matzuk, M. M. (2006). Non-invasive genetic diagnosis of male infertility using spermatozoal RNA: KLHL10 mutations in oligozoospermic patients impair homodimerization. *Hum. Mol. Genet.* **15**, 3411-3419.

Yue, L. and Spradling, A. C. (1992). hu-li tai shao, a gene required for ring canal formation during Drosophila oogenesis, encodes a homolog of adducin. *Genes Dev.* **6**, 2443-2454.